Torregrosa, AJ.; Broatch Jacobi, JA.; Margot, X.; Garcia Tiscar, J. (2016). Experimental methodology for turbocompressor in-duct noise evaluation based on beamforming wave decomposition. Journal of Sound and Vibration. 376:60-71. doi:10.1016/j.jsv.2016.04.035.

Experimental methodology for turbocompressor in-duct noise evaluation based on beamforming wave decomposition

A. J. Torregrosa[a], A. Broatch[a,*], X. Margot[a], J. García-Tíscar[a]

[a] *CMT - Motores Térmicos, Universitat Politècnica de València*
Camino de Vera, 46022 Valencia, Spain

Abstract

An experimental methodology is proposed to assess the noise emission of centrifugal turbocompressors like those of automotive turbochargers. A step-by-step procedure is detailed, starting from the theoretical considerations of sound measurement in flow ducts and examining specific experimental setup guidelines and signal processing routines. Special care is taken regarding some limiting factors that adversely affect the measuring of sound intensity in ducts, namely calibration, sensor placement and frequency ranges and restrictions. In order to provide illustrative examples of the proposed techniques and results, the methodology has been applied to the acoustic evaluation of a small automotive turbocharger in a flow bench. Samples of raw pressure spectra, decomposed pressure waves, calibration results, accurate surge characterization and final compressor noise maps and estimated spectrograms are provided. The analysis of selected frequency bands successfully shows how different, known noise phenomena of particular interest such as mid-frequency "whoosh noise" and low-frequency surge onset are correlated with operating conditions of the turbocharger. Comparison against external inlet orifice intensity measurements shows good correlation and improvement with respect to alternative wave decomposition techniques.

Keywords: Turbocharger, Aeroacoustics, Noise map, Automotive, Whoosh, Surge

1. Introduction

As competition from alternative-powered vehicles and environmental concerns increase, traditional internal combustion engines for automotive applications are facing tougher scrutiny by regulators and consumers.

Requirements for lower pollutant emissions (such as NO_x, CO, particulate matter, etc.) and higher efficiency (in order to reduce production of CO_2) are becoming more restrictive. An overview of these upcoming regulations is available from Op de Beeck et al [1]. Consumers are also sensitive to the NVH (noise, vibration, harshness) performance of vehicles, and to the adverse impact of automotive emissions (including noise pollution), as shown by Brizon and Bauzer [2].

In order to match these expectations automotive engines are heavily downsized in terms of displacement and number of cylinders. However, these engines are still required to provide equivalent levels of torque and power output, so that turbocharger performance has to increase. Further discussion on downsizing, turbocharging and its importance to meet stricter emission policies is available in the work of Schumann et al [3].

However, it should be noted that this strategy is not without consequences. Stoffels and Schroeer [4] have shown how at certain operating conditions a downsized engine can radiate higher noise levels than its larger displacement equivalent.

An important contributor to engine noise radiation is the turbocharger compressor, as it operates at conditions close to its limiting surge line [5] due to increased turbocharging requirements.

However, increased noise *quantity* is not the only concern: it is also very relevant to take into account the *frequency* in which the noise increases, regarding attenuation possibilities as well as psychoacoustic perception of "sound quality" by the consumer, as shown in the above cited study [2] and in that of González et al [6].

*Corresponding author. Tel.: +34 963 877 650, email: abroatch@mot.upv.es

In this paper, a methodology is proposed to evaluate the noise emission of the compressor through its inlet and outlet pipes in selected zones of the compressor map of operating conditions. It allows a simple and clear visualization of noise phenomena and their frequency distributions at all possible operation points of the turbocharger system.

Although compressor manufacturers sometimes provide these noise maps [7], they usually refrain from providing an adequately referenced and step-by-step methodology to reproduce them.

Reviewing the existing literature on turbocompressor noise a variety of very different measurement techniques can be found, from the two-sensor, in-duct approach of Tiikoja et al [8] to simple single-sensor pressure levels and external commercial noise-meters [9].

However, these works focus on the research of different phenomena (transmission loss [8], effect of flow incidence angle [9], sound generation by rotating stall [10], source characterization [11], etc.), not on the acoustical methodology itself nor on the particular setup considerations and restrictions that each measurement technique imposes.

This work wishes to address the shortcomings of the existing literature by proposing an experimental methodology and discussing the details of its theoretical background, its implementation, its range of application, and the processing required to produce standardized results.

In order to provide some illustrative results, the methodology proposed in this paper has been applied to a series of experimental tests in a flow bench where a small automotive turbocharging group has been installed. Applicability of the methodology and comparison with other methods is also discussed.

2. Theoretical methodology

2.1. Sound intensity in flow ducts

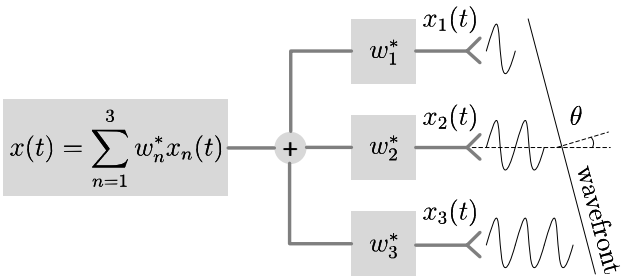

Figure 1: Diagram of a narrowband beamformer with three elements tuned to a Direction of Arrival (DOA) of θ.

While it is possible [9] to rely on a single sensor to measure the scalar *sound pressure level* (SPL) of the flow at a certain location of a duct, more sophisticated approaches are needed to estimate the *sound intensity level* (SIL) that is propagating through the duct.

It is important to consider that the scalar magnitude of sound pressure level at a point can be influenced by the precise geometry of that section and by nodes and reflections that may occur in the duct, whereas sound intensity is a vectorial magnitude that remains almost constant along the duct (except for small dissipation losses), and thus is a more robust indicator of noise emission.

The basis of the intensity measurement methods is to consider that the pressure signal $x(t)$ measured at a given point of a duct is the linear superposition of a pressure wave x^+ travelling downstream and another pressure wave x^- travelling upstream (sometimes referred to as forward and backward waves, respectively [12]) so that:

$$x(t) = x^+(t) + x^-(t) \tag{1}$$

By comparing the pressure information at two or more spatial positions it is possible to infer how the waves are propagating along the duct in each direction; this information is not available by means of a single sensor.

When using this wave decomposition approach, the sound intensity is commonly estimated following the definition proposed by Morfey [13] and successfully derived by Dokumaci [14] from physical principles [15, 16, 17] :

$$I = \frac{1}{\rho a}\left(|\mathbf{X}^{+}|^{2}(1+M)^{2} - |\mathbf{X}^{-}|^{2}(1-M)^{2}\right) \tag{2}$$

Here $\mathbf{X}^{+}$ and $\mathbf{X}^{-}$ are, respectively, the complex spectra of the downstream and upstream pressure waves, ρ is the mean density, a the mean sound speed, and M the mean Mach number of the flow.

2.2. *Wave decomposition*

There exist several techniques to perform the required wave decomposition. The beamforming method provides a way to mathematically tune the sensitivity of the overall system in order to isolate the downstream and upstream information of the acquired signal. A scheme for a narrowband beamformer can be found in Fig. 1.

For a more intuitive understanding of the beamformer, one can consider its transmitting equivalent: a phased array emitter where the same signal $x(t)$, with its phase shifted by a quantity w_n^*, is fed to an n-element linear array of fixed transmitters, forming a plane wave emitted in the θ direction which can be steered at will adjusting each w_n^*.

The approach in this paper is the inverse: by tuning the weights w_n^* that multiply each recorded pressure signal $x_n(t)$ the pressure wave coming from the direction of arrival (DOA) θ that we are interested in may be resolved. Details can be found in [18].

The extension to a wideband beamformer is relatively straightforward [19]. First the Fast Fourier Transform (FFT, denoted by $\mathcal{F}$) of the recorded pressure signals is computed:

$$\mathbf{X}_n(f_k) = \mathcal{F}\{x_n(t_k)\} \tag{3}$$

Subscript k indicates that the signal is acquired at discrete time steps. The described narrowband procedure is then followed for each discrete frequency to finally obtain the desired signal through the inverse transform:

$$x(t) = \mathcal{F}^{-1}\left\{\mathbf{w}^{H}(f_k)\,\mathbf{X}(f_k)\right\} \tag{4}$$

Here, $\mathbf{X}(f_k)$ is the $k \times n$ matrix of transformed signals and $\mathbf{w}^{H}(f_k)$ is the matrix of weights for each frequency. In order to compute the optimal weights for the desired DOAs ($\theta = -90^{o}$ for downstream and $\theta = 90^{o}$ for upstream waves, assuming a typical flow DOA of $\theta = 90^{o}$), several schemes can be used.

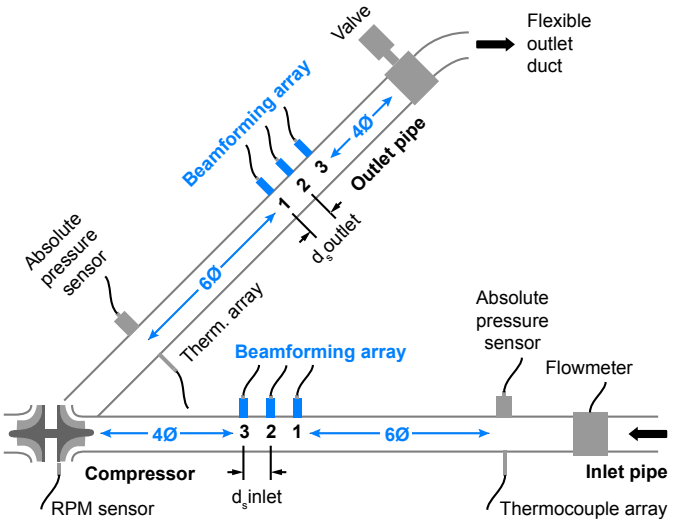

Figure 2: Scheme of the proposed turbocharger instrumentation setup, highlighting in color the three-sensor beamforming arrays and their clearance requirements.

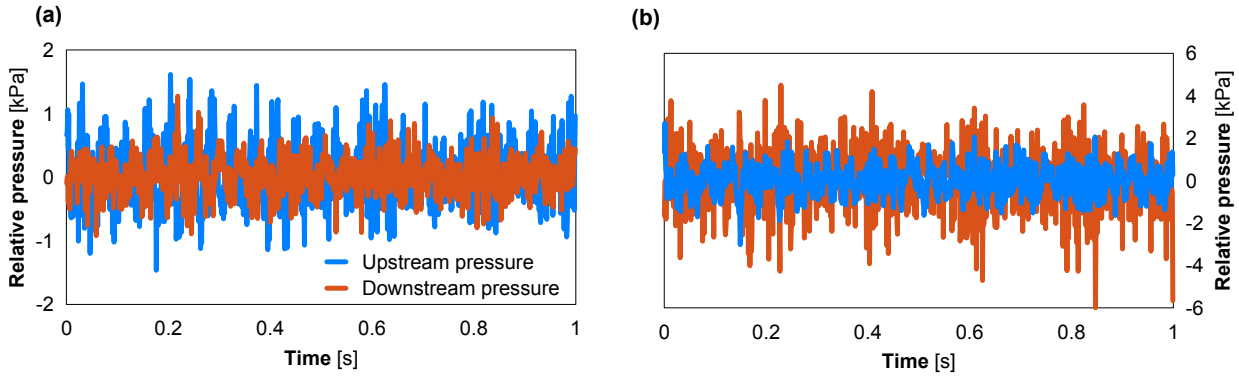

Figure 3: Sample result of the decomposed pressure; at the inlet (a) the amplitude of the pressure wave travelling downstream (towards the compressor) is smaller than the one coming from the compressor; the reverse situation occurs at the outlet (b).

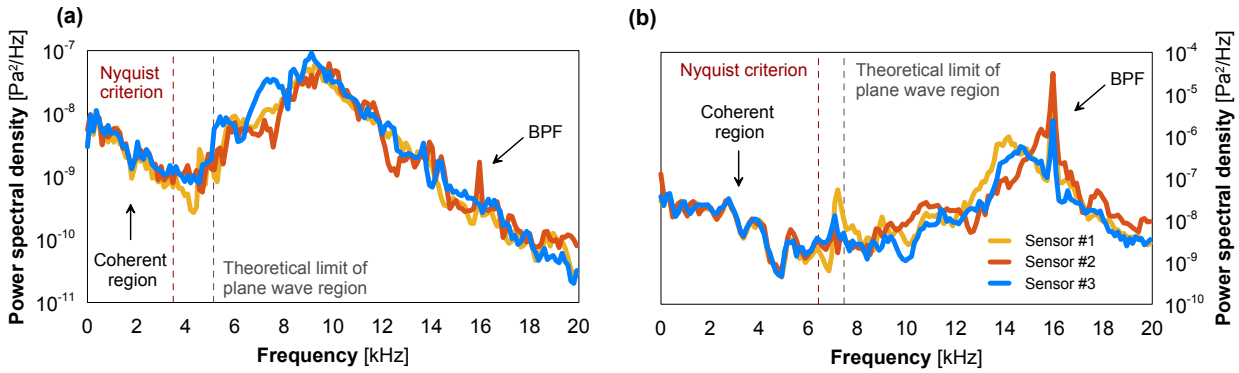

Figure 4: Sample of raw inlet (a) and outlet (b) pressure power spectral densities (at 160 krpm and 60 g/s), including frequency limitations described in equations 6 and 7. The characteristic blade pass frequency can also be identified, specially in the outlet spectra.

For this study a Linearly Constrained Minimum Variance (LCMV) beamformer was used, a well established procedure, which aims at minimizing the overall output power (variance) of the signal, while maintaining unitary gain in the precise desired direction.

While several beamforming strategies and implementations are available, Appendix A offers a simple guide on how to compute $\mathbf{w}^H(f_k)$ and thus $\mathbf{X}^+$ and $\mathbf{X}^-$ using this particular approach. Figure 3 shows the result of this decomposition in the time domain.

Information on its application, including a comparison of various of these schemes against simulated and experimental data is available in [12]. Further discussion on the performance on the selected beamforming algorithm and the applicability of the wave decomposition approach is presented in section 5.

3. Experimental procedure

3.1. Turbocharger instrumentation

The correct design and installation of the fast pressure sensor arrays is a critical part of the experimental setup.

Ideally, the sensors should be mounted flush (with water-cooled adapters if necessary) in straight pipes, with diameters adjusted to preserve the cross sectional area of the adjacent duct in order to avoid complex structures caused by singularities.

As a further measure, enough straight clearance should be left before and after the array (as shown on figure 2), to ensure essentially plane wave flow at the measurement section [15]. There should be a minimum of 6 diameters upstream of the array and a further 4 diameters downstream, as recommended in [20].

When placing the transducers, it is important to avoid the 1/5 and 1/3 nodes of the established standing wave pattern [21]. Also, a compromise in the spacing d_s between them must be reached, taking into consideration errors in the low-frequency [22] and high-frequency [23] bands.

In particular, it should be noted that spatial aliasing effects will occur above the Nyquist frequency imposed by the spacing d_s. The time for a wave with DOA θ and speed a to travel between two consecutive sensors spaced by a distance d_s is:

$$T_d = \frac{d_s \sin\theta}{a} \tag{5}$$

This imposes a Nyquist-type frequency criterion, as the measured wave frequency f_n should be maximum half the frequency $f_d = 1/T_d$ naturally associated with T_d to ensure that no high frequency spatial aliasing effects are present:

$$f_n \leq \frac{f_d}{2} = \frac{1}{2T_d} = \frac{a}{2d_s \sin\theta} = \frac{a}{2d_s} \tag{6}$$

A further restricting phenomenon is the acoustic mode propagation. As the beamforming method proposed is based on the assumption of one-dimensional wave propagation, it will become unreliable with the onset of 3D effects.

According to Eriksson [24], it may be assumed that waves in a circular duct propagate in a planar fashion (i.e., pressure is constant in every cross-sectional area of the duct) below a cut-off frequency of:

$$f_a = 1.84 \frac{a}{\pi D} \sqrt{1 - M^2} \tag{7}$$

Here, a is the sound speed, D the duct diameter and M the mean Mach number. At higher frequencies, the so-called first asymmetric mode will start to propagate, thus rendering the assumption of one-dimensional propagation invalid.

Special care should be taken when computing limiting frequencies f_n and f_a as they are not constant but dependent on the operating condition, since some of their components vary with temperature and mass flow. Figure 4 shows both limits for a certain operating point.

As the figure shows, the Nyquist criterion accurately pinpoints where differences between sensors start to grow, and it is clearly a more restrictive criterion than the acoustic mode onset. This limit should be properly computed for each condition when multi-sensor decomposition techniques are used.

Also, figure 4 shows other phenomena, for instance the peak related to the passing of each rotor blade, usually known as Blade Passing Frequency (BPF) in the literature [25], which is marked as such in the figure:

$$\text{BPF} \sim 160\,\text{krpm} \,/\, 60\,\frac{\text{s}}{\text{min}} \times 6\,\text{main blades} \sim 16\,\text{kHz} \tag{8}$$

It is also important to note that the closer the sensors are mounted together for increasing the f_n limit, the poorer the spatial resolution of low frequency waves will be, as the wavelengths $\lambda = a/f$ become too long and the difference between consecutive sensors decreases below the noise threshold. This effect is intrinsically related to each particular sensor model, but it must be considered if very low frequencies are of interest.

Finally, it is essential to ensure that the response of the three sensors of each array is coherent. Before mounting the sensors in the final linear array form, they should be mounted radially in the same section of a duct and individually calibrated, to ensure that the difference between sensors is not due to individual transducer differences, but only to wave propagation.

In this case, the calibration is performed in an impulse test rig (described in detail in [26]) so as to obtain a clear reference pressure wave in all sensors. Both the time and frequency responses are observed, and both the amplifier offset and gain are adjusted to find the best match. An example can be seen on figure 5.

In addition to the fast pressure sensors data, more information is required to compile the compressor operating conditions map. These maps are usually presented as plots of the operation points on a total-to-total pressure ratio (Π_{TT}) versus corrected air mass flow ($\dot{m}^*$) axes.

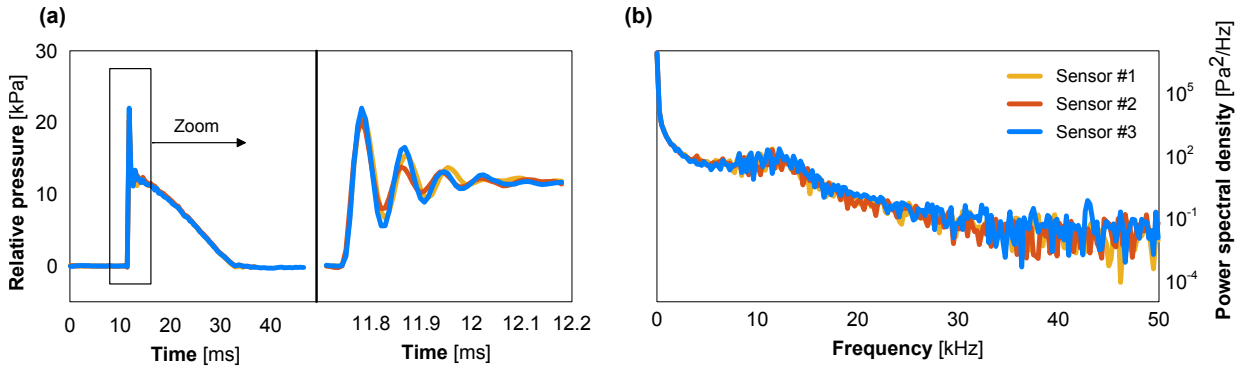

Figure 5: Results of the calibration of the outlet sensors in an impulse test rig, showing a pressure measurement match in both time (a) and frequency domains (b).

3.2. Steady state measurements

The usual approach for measuring the operating points of the compressor map involves reducing the air flow by progressively closing the back-pressure valve (shown in figure 2) until the desired air mass flow is reached, while the turbine power is adjusted to preserve a given corrected compressor speed (N^*) and to achieve stable operation conditions.

Eventually the compressor blades will begin to stall, until a deep surge condition is reached, as shown in the left plot of figure 6. In order to avoid this destructive condition, the valve will be opened again and another constant corrected regime line will be measured, until the desired region of the compressor map is completely covered.

Several reference conditions can be selected when correcting the speed and the air mass flow; in this study the mean sea level standard day (defined as one of 15°C of temperature and 1 atm of pressure) of the International Standard Atmosphere will be used:

$$\dot{m}^* = \dot{m}\frac{101325}{p_T}\sqrt{\frac{T_T}{288.15}} \qquad N^* = N\sqrt{\frac{288.15}{T_T}} \tag{9}$$

Here, p_T and T_T refer to the compressor inlet total pressure and temperature, respectively. These are calculated with the air mass flow and the cross sectional area of the inlet duct, using the continuity and ideal gas relations and assuming adiabatic flow.

Here R denotes the air-specific ideal gas constant and ρ, P, T and V the density, pressure, temperature and flow speed in the duct, respectively. With A denoting the cross sectional area, and c_p the air-specific heat capacity, it follows that for both ducts:

$$\rho = \frac{p}{RT} \quad V = \frac{\dot{m}}{\rho A} \quad T_T = T + \frac{V^2}{2c_p} \quad p_T = p\left(\frac{T_T}{T}\right)^{\frac{\gamma}{\gamma-1}} \tag{10}$$

Figure 6 (right) shows the recorded data points of the compressor map, after computing the total-to-total pressure ratio and applying the standard day correction.

3.3. Surge limit characterization

When measuring a turbocharger operation map, it is particularly important to characterize accurately the surge limit, especially when an acoustic evaluation is sought out [27].

In order to measure different mass flows, the back-pressure valve is usually gradually closed until a certain surge criterion is met, and then opened to avoid damaging the turbocharger. Several surge criteria for centrifugal turbo-machines have been proposed in the literature, for tests on flow benches [27] and on engine test rigs [28].

Among these, the average of the power spectrum of a single pressure sensor in the 0 to 20 Hz range, shown by Galindo et al [27] to be a good surge indicator, was computed once for discrete time steps ΔT of 0.5 seconds. The

result of the averaging process provides a clear indication of the deep surge onset, as marked in figure 6 (left) with a solid line.

$$\mathbf{X}_T = |\mathcal{F}\{x(t)\}|^2 \,,\; t \in [t_T, t_{T+1}] \tag{11}$$

To obtain the required near-surge data points to be displayed on the compressor map, represented by ■ in the right plot of figure 6, a one second average of all recorded data was computed one second before surge as indicated by the dashed lines of the left plot.

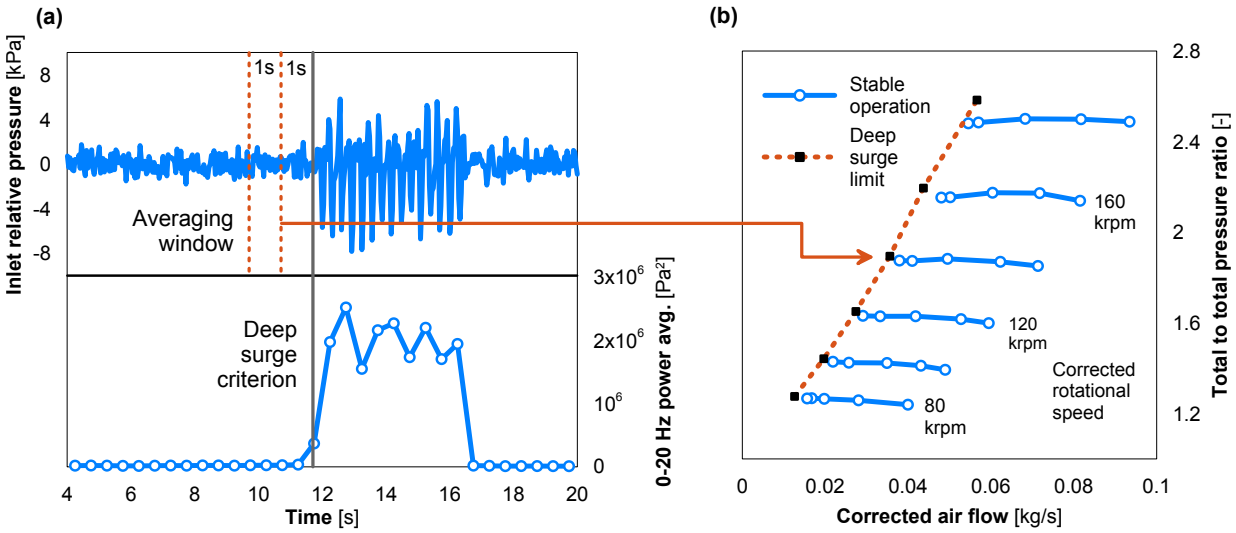

Figure 6: Sample of precise determination of the deep surge limit (a) for each air flow limit point of a compressor map (b), including temporal evolution of the raw relative pressure recorded by one piezoelectric sensor and correlation between the frequency content in the 0-20 Hz band and deep surge onset.

3.4. Signal post-processing: maps and spectrograms

In addition to the intensity spectra determined for each operating point, further results can be obtained by applying an interpolation procedure to the spectra associated with all the points tested.

For instance, it is possible to calculate the overall level of sound intensity for a given frequency range at each operating point i of the compressor operating map. The sound intensity level in a characteristic band (between f_1 and f_2) can be calculated for each point as:

$$L_i = 10 \log_{10}\left(10^{12} \sum_{f=f_1}^{f_2} I(f)\right) \tag{12}$$

Once that several L_i levels have been measured for different conditions of a selected map region, a cubic spline interpolation function $\Phi_{f_1-f_2}$ is used to project the data onto a much more fine and regularly spaced grid, allowing the representation of a map of noise intensity across the measured region of the compressor map, as shown in figure 7.

These "noise maps" synthesize the information of the acoustic output of a frequency band of interest in a simple and visual form, allowing an easy estimation of the noise emission in any operating conditions, even if these have not been specifically measured.

Expanding on the necessity of analyzing the frequency content evolution as the operating conditions of the compressor change, a different approach can be used whereby the measured discrete information can be compiled to estimate a continuous spectrogram.

This is accomplished by sequentially performing the previous map processing for a number N of much smaller frequency bands of width Δf, resulting in a collection of N interpolation functions $\Phi_{f_j-f_{j+1}}$, where $f_{j+1} - f_j = \Delta f$.

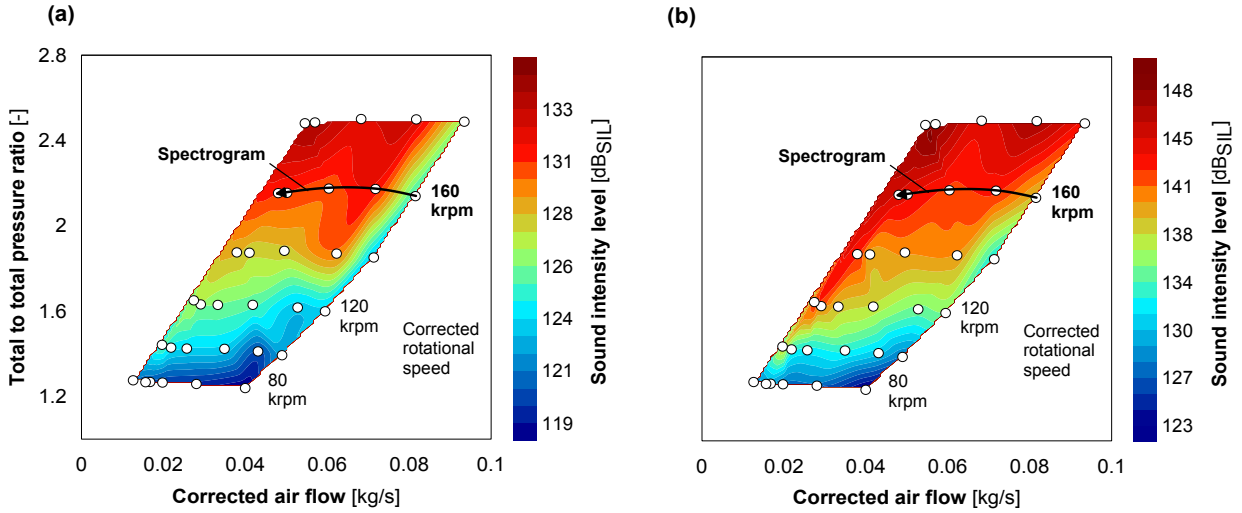

Figure 7: Sample of noise level for both inlet (a) and outlet (b) in the 1 – 3 kHz band obtained through the processing described in subsection 3.4, including the measured data points (○) and the paths later expanded as spectrograms shown in figure 8.

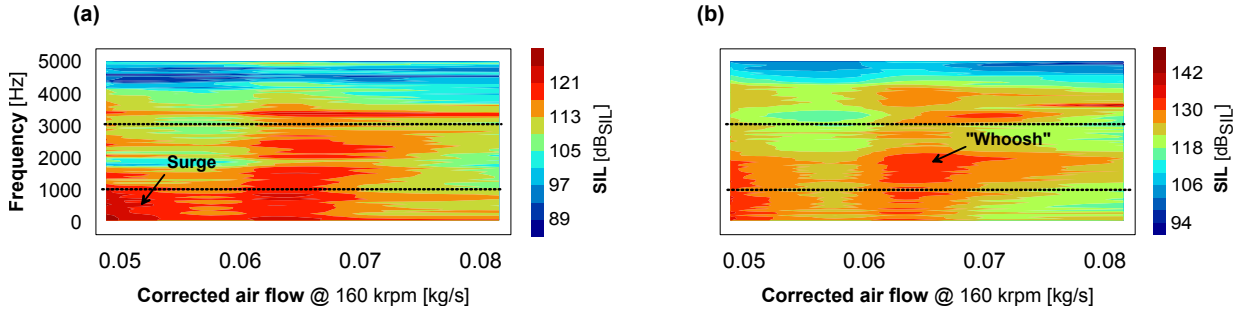

Figure 8: Sample of spectrograms for both inlet (a) and outlet (b) calculated using the procedure outlined in subsection 3.4, following the 160 krpm paths marked in figure 7. The 1–3 kHz band selected for the maps in figure 7 is highlighted, along with some particular flow phenomena discussed in section 4.

Using these functions, the intensity levels $\mathbf{L}$ on each small frequency band k are interpolated for a set of M pairs of the compressor map coordinates, such that:

$$\mathbf{L}_j = \Phi_{f_j - f_{j+1}}(\dot{\mathbf{m}}^*, \mathbf{\Pi}_{\mathrm{TT}}) \tag{13}$$

An estimation of the spectrogram $\mathbf{S}$ that would be obtained in a quasi-stationary measurement by following the set of operation conditions $(\dot{\mathbf{m}}^*, \mathbf{\Pi}_{\mathrm{TT}})$ pairs can then be compiled gathering the levels $\mathbf{L}_j$. Choosing one coordinate of the set of pairs (in this case $\dot{m}^*$) as reference for the X axis:

$$\mathbf{S}(f_j, \dot{m}^*) = \begin{bmatrix} \mathbf{L}_1(\dot{m}_1^*) & \dots & \mathbf{L}_1(\dot{m}_M^*) \\ \vdots & \ddots & \vdots \\ \mathbf{L}_N(\dot{m}_1^*) & \dots & \mathbf{L}_N(\dot{m}_M^*) \end{bmatrix} \tag{14}$$

Thus the sound intensity level value $\mathbf{S}$ for each m^* and each frequency band j can be plotted. An example of this processing for frequencies between 50 and 5000 Hz binned with $\Delta f = 50$ Hz is presented on figure 8, where coordinates $(\dot{\mathbf{m}}^*, \mathbf{\Pi}_{\mathrm{TT}})$ correspond to the 160 krpm iso-speed line highlighted in figure 7.

4. Setup and results of a sample case

In order to illustrate the methodology presented in this paper, the evaluation of a small automotive turbocompressor was carried out in a flow bench, configured as shown in figure 2.

Kistler type 7031 piezoelectric transducers were used for the inlet duct; the outlet duct was fit with type 6031 transducers due to available stock. An array spacing $d_s = 32$ mm for the outlet and $d_s = 50$ mm for the inlet was selected, allowing for a safe upper limit in terms of the spatial Nyquist criterion f_n of ~6000 and ~3500 Hz respectively (precise values depend on the conditions of each point).

The variables needed in order to characterize the map point (mass flow, speed, temperatures and pressures) were averaged during 30 seconds, while the six piezoelectric sensors acquired 10^5 pressure samples during one second using a Yokogawa digital recorder.

Pressure signals on recorded points (shown in figure 6) were then processed according to the proposed methodology. Samples of the final results are presented in figures 7 and 8.

Figure 7 shows the 1 – 3 kHz sound intensity level distribution across selected operating conditions, approximately between maximum efficiency and the measured surge limit.

Noise in this frequency band is sometimes designated as "whoosh" noise in the literature, and is of particular concern for automotive manufacturers, as the user may perceive negatively this particular frequency. Indeed, the user expects a low frequency engine sound instead of a high-pitched one.

Another point of concern that has been identified in the results is that the relevance of this particular phenomenon extends far from the surge region and well into the expected engine operation region.

In fact, looking at either the 160 krpm line on figure 7 or at the expanded spectrograms of this line in figure 8 where this band has been marked, there is a local maximum in this band between 60 and 70 g/s. For the 180 krpm points on the map of figure 7, the "whoosh" noise may be heard even for up to 80 g/s mass flow rate.

Apart from "whoosh", both spectrograms show a clear rise in low frequency content when the mass flow is reduced and surge conditions start to appear, even if deep surge conditions have not yet been reached. This is consistent with spectrograms measured experimentally by Galindo et al [29].

Furthermore, this kind of low frequency band may be plotted and its distribution compared with other bands, as shown in figure 9 where three different frequency limits have been applied to equation 12 during signal processing.

Compared with the global distribution of sound intensity in the plane wave range (Fig. 9 a), the "whoosh noise" band (Fig. 9 b) appears to be more prevalent at higher pressure ratios, while the low frequency content (Fig. 9 c) is characteristic of surge onset.

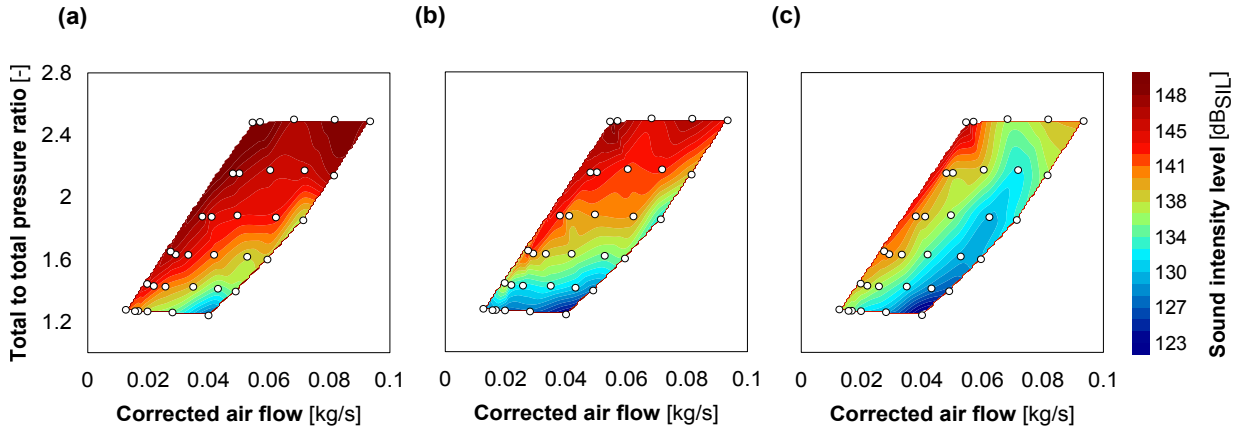

Figure 9: Outlet intensity maps computed at different frequency ranges: a general view (20 Hz – 5 kHz) of the plane wave range global intensity (a); the characteristic band (1 kHz – 3 kHz) of the "whoosh noise" (b), and a narrow low frequency band (20 Hz – 200 Hz) indicative of deep surge onset (c).

These observations match the trends observed in the literature [30, 31, 32]. Other frequency bands could be mapped in a similar manner, and spectrograms estimated for different map paths with no need to repeat the experimental measurements, in order to investigate other phenomena of interest or to test several candidates for actual engine operating lines.

5. Discussion

5.1. Improvements over standard wave decomposition techniques

Beamforming is a wide term that describes a variety of multi-sensor spatial filtering techniques. In fact, the classical Seybert two-microphone method (TMM) [23] commonly used to decompose pressure waves can be classified as an equivalent to a two-sensor delay-and-sum (DS) beamformer [12].

DS beamformers are robust since they are data independent, i.e. they do not require assumptions about statistical properties of the incoming signal. However, when some statistical assumptions about the incoming signal are made, other techniques can be used to optimize output [18]. These are referred to as statistically optimum beamformers.

In this work the well established LCMV beamformer algorithm [33] has been selected, which assumes that signals and noise are sufficiently uncorrelated. Its main advantage lies in its optimization of the signal-to-noise-plus-interferences ratio (SINR) at the beamformer output, while avoiding the need for a reference signal or for additional reference channels, as is the case for other statistical optimum techniques [18].

However, care should be taken to ensure that forward, backward waves and noise are sufficiently uncorrelated, as otherwise some degradation of the performance may occur. In the authors' experience these negative conditions can be consistently avoided in turbocharger in-duct measurements when the instrumented pipes and the sensor arrays comply with the suggested lengths and spacings.

In the sample case presented here the correlation coefficients of forward and backward waves were consistently below 0.5, as measured by a data independent classical DS beamformer. In any case, sensor spacing of more than half the hydraulic diameter of the pipe should ensure that the turbulent noise is uncorrelated between sensors [34].

Hence, the use of the LCMV algorithm should provide a better isolation against interfering signals and turbulent noise, improving the ability of the proposed method to correlate with other turbocharger acoustic characterization approaches such as the measurement of the inlet orifice noise, usually performed in anechoic chambers.

To test the feasibility of this correlation, in-duct data gathered from a turbocharger installed in an anechoic chamber was processed using the suggested LCMV beamforming algorithm and the classical two-microphone method (TMM), and compared against that obtained by an omni-directional free-field microphone located 10 cm away from the inlet orifice of the compressor.

Since the anechoic chamber eliminates sound reflections, the free-field intensity equation can be used to estimate the intensity I from the pressure signal P measured by the microphone, using ambient pressure p and temperature T to calculate acoustic impedance Z:

$$I = \frac{P^2}{Z} = \frac{P^2}{\rho a} = \frac{P^2}{\rho \sqrt{\gamma R T}} = \frac{P^2 R T}{p \sqrt{\gamma R T}} \tag{15}$$

Plot a) of Fig. 10 shows this comparison: although both methods offer a good correlation, the LCMV algorithm yields a better coefficient of determination R^2 after performing a linear regression. Note that the plotted intensities are restricted to the 250–2650 Hz range in order to compare with the data from an engine test cell reproduced in plot b).

This second correlation is shown to assess the performance of the proposed method in a partially conditioned engine test cell described in [35]. In this second case, in-duct acoustic intensity was used on the modified inlet line of a turbocharged engine, and data was reprocessed comparing again the LCMV and TMM approaches.

Since free-field conditions could not be guaranteed in the engine test cell, a commercial B&K intensity probe was used at the inlet orifice instead of the free-field microphone. Data from this probe was gathered using a B&K Pulse system.

In these demanding engine conditions with highly pulsating flow, the difference in terms of R^2 between the LCMV and TMM wave decomposition methods increased, thus suggesting that the use of the LCMV beamformer effectively improves the robustness of the in-duct measurement, especially when correlation with orifice measurements is desired.

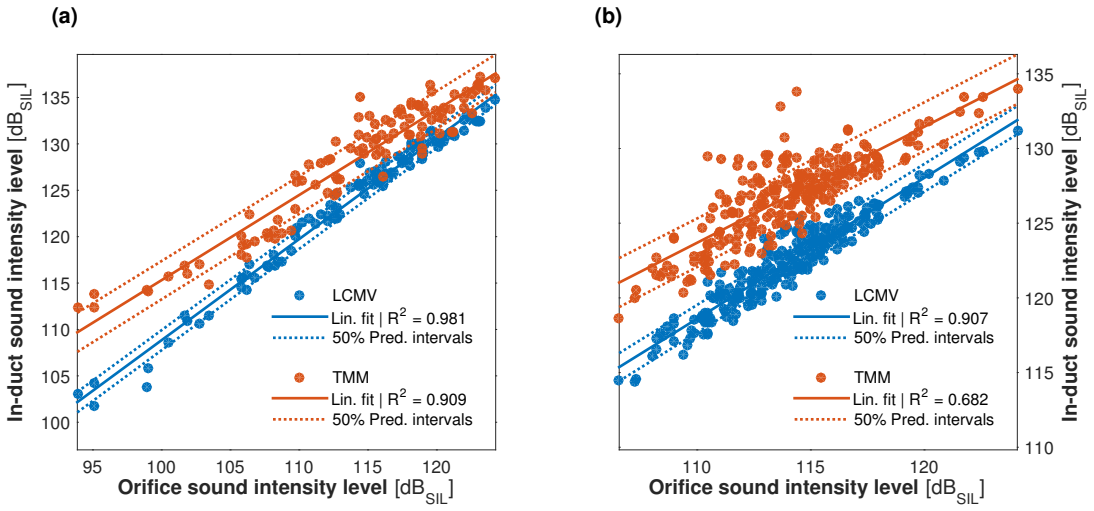

Figure 10: Correlation between simultaneous measurements of in-duct sound intensity (computed with both LCMV and TMM methods) and orifice sound intensity. In case (a) measurements were performed with an isolated turbocharger inside an anechoic chamber whereas in case (b) measurements were made in an engine test cell.

5.2. Applicability of the proposed methodology

It is well established in the literature that the particular details of the inlet and outlet geometries, especially of the inlet section immediately upstream of the compressor, have a great influence on the unstable behaviour of the flow [36, 37]. Geometric changes in the pipe geometry such as elbows, tapered ducts, volumes, nozzles, whirl-inducing devices, ported shrouds, etc..., modify the compressor performance, pressure fluctuations, surge onset mass flow, deep surge frequency and thus, its acoustic behaviour.

For this reason, in order to obtain meaningful in-duct intensimetry results, it is important to stress the importance of testing the turbocharger integrated within the final geometric design line. Indeed, the pipe geometry of the turbocharger must be at least representative of the intended design in the sections close to the compressor inlet and outlet ports. Otherwise, if the turbocharger were to be tested with simplified straight test pipes, the flow pattern would be significantly different from the flow in real operating conditions, and this naturally affects the acoustics. Consideration of both inlet and outlet forward and backward intensity components is thus required when the total in-duct intensity is calculated, especially when the intention is to account for sound radiation from the ducts and not only from the turbocharger itself.

The proposed method allows the fitting of representative compressor terminations, including complex duct geometries and also actual line components such as air boxes, filters, flow meters, etc., only requiring that a straight instrumented section is included where convenient. Measurement inside standard engine test cells is also possible without the need for acoustical conditioning, as opposed to external measurements that are negatively affected by reflection and reverberation.

Also, though there is no guarantee that the isolated pressure signals coming from the compressor (x^- in the inlet and x^+ in the outlet) are free of information that is dependent on the particular duct geometry, these have proven to be a valuable byproduct of this method, in particular for use in CFD simulations. Indeed, it is known that boundary conditions for acoustic CFD calculations have to be defined as anechoic in order to avoid having to model components such as valves, flexible ducts, etc..., the inclusion of which complicates the mesh geometry and increases computational time. Since the decomposed signals enhance the pressure spectral content coming from the compressor with respect to the interferences of reflections and uncorrelated turbulent noise, they have been used as alternative to anechoic boundary conditions in CFD simulations with good results [38].

Note however that the decomposed forward and backward pressure waves do not characterize the true reflection-free acoustic source represented by the compressor. This characterization, including two-port modelling, transmission loss, etc... would require the fitting of loudspeakers, anechoic terminations, etc... as shown for instance in the work of Kabral et al. [39]. For this a complex test rig would have to be set up, and in many a case it would not be realizable, as is the

case for instance for the on-engine application described in [35], where the outlet of the turbocharger is connected to the engine manifold, and thus not accessible for modification.

Another limitation of the wave decomposition methods is that they are confined to the plane wave region of the spectrum. While this region encompasses frequencies of interest for automotive turbochargers [7], frequencies beyond the plane wave range are also interesting, especially from a fluid mechanics point of view.

To the authors' knowledge no definitive method has yet been established to measure sound intensity in ducts with flow when 3D effects are present. However, the procedure presented by Hynninen and Åbom [34] is a promising empirical approach that could be adapted to extend the useful range of the procedure presented in this paper.

5.3. Future work

Coupled measurements of the radiated noise from the whole engine and in-duct turbocharger noise would be of great interest to assess how masking affects different frequency ranges, especially in regard of the whoosh noise problem. Two approaches can be considered to pursue this objective. One option involves the installation of an engine in the anechoic chamber, where free-field microphones could be used to assess the noise output without reverberation disturbances. The other would involve the use of a novel acoustical particle velocity sensor, which should be more robust when measuring in near field conditions, so that it could be used in a normal, non-anechoic engine test cell. A promising sample measurement of turbocharger whoosh noise radiation using the latter approach can be found in [35].

Another interesting future development will be the application of the in-duct methodology proposed in this paper for testing different geometry modifications, in order to assess if possible improvement in terms of noise can be obtained without deteriorating the performance in terms of efficiency and surge range.

6. Conclusions

In this paper a detailed experimental methodology for the noise evaluation of turbocharger compressors in flow benches [40] or engine test cells [35] is proposed and demonstrated. It is based on a robust in-duct acoustical beamforming technique that resolves the plane wave range sound intensity, by decomposing the total pressure signal into its forward and backward components.

When used to evaluate the acoustic intensity of the noise generated by the compressor, the proposed signal processing provides easy to interpret visual representations in the form of noise maps in selected frequency bands of interest, and estimated spectrograms of operating paths. This can provide guidelines for the evaluation of strategies to counter or avoid certain adverse noise phenomena.

The examples presented above illustrate how this technique allows detecting known acoustical phenomena for a centrifugal compressor, such as medium frequency "whoosh noise" and low frequency surge onset, as well as mapping the corresponding noise distribution and relevance at different operating conditions of the turbocharger.

In addition to presenting the detailed measurement and signal processing steps, this paper stresses the importance of taking into account restrictive factors such as calibration, sensor setup clearances and locations, frequency aliasing effects and ranges in which theoretical assumptions hold in order to obtain robust and reproducible results.

A discussion has been presented to demonstrate the improvements obtained with the proposed method over usual procedures and its good correlation with orifice noise measurements. Some remarks about its applicability and future activities that may be of interest have also been included.

In summary the technique presented here should provide researchers who need to evaluate turbocharger compressor noise emission with a means to focus their efforts on the acoustical phenomena, instead of on the measurement itself, thus allowing to further advance knowledge on this topic.

Acknowledgements

The equipment used in this work has been partially supported by the Spanish Ministerio de Economía y Competitividad through grant no. TRA2012-36954 and by FEDER project funds "Dotación de infraestructuras científico técnicas para el Centro Integral de Mejora Energética y Medioambiental de Sistemas de Transporte (CiMeT), (FEDER-ICTS-2012-06)" framed in the operational program of unique scientific and technical infrastructure of the Spanish Ministerio de Economía y Competitividad.

Appendix A. LCMV beamforming procedure

This appendix proposes a step by step guide to compute the desired $\mathbf{X}^+$ and $\mathbf{X}^-$ decomposed pressure spectra required in equation 2 of subsection 2.1, using a LCMV (Linearly Restricted Minimum Covariance) strategy as presented by Verdú [41].

Recall that decomposed signals for each frequency f_k are obtained by weighting the transformed measurement matrix $\mathbf{X}(f_k) = [X_1 X_2 X_3] = \mathcal{F}\{[x_1 x_2 x_3]\}$ as follows:

$$\mathbf{X}^+(f_k) = \mathbf{w}^{+H}\mathbf{X}(f_k) \tag{A.1}$$

$$\mathbf{X}^-(f_k) = \mathbf{w}^{-H}\mathbf{X}(f_k) \tag{A.2}$$

It can be shown that the corresponding weights for filtering the downstream and upstream signals are obtained for each frequency f_k by:

$$\mathbf{w}^+ = \mathbf{g}^+\left[\Sigma_x^{-1}\,\mathbf{A}^H(\Theta)\left[\mathbf{A}^H(\Theta)\,\Sigma_x^{-1}\,\mathbf{A}^H(\Theta)\right]^{-1}\right] \tag{A.3}$$

$$\mathbf{w}^- = \mathbf{g}^-\left[\Sigma_x^{-1}\mathbf{A}^H(\Theta)\left[\mathbf{A}^H(\Theta)\,\Sigma_x^{-1}\,\mathbf{A}^H(\Theta)\right]^{-1}\right] \tag{A.4}$$

Where $g^+ = [1\ 0]^T$ and $g^- = [0\ 1]^T$ are the desired response vectors (unitary gain in one direction and zero gain in the opposite). Σ_x denotes the covariance matrix. For a certain discrete frequency f_k, using the expected value E:

$$\Sigma_x(f_k) = E[\mathbf{X}(f_k)\,\mathbf{X}^H(f_k)] \tag{A.5}$$

The constraints matrix $\mathbf{A}(\Theta) = [\mathbf{a}^+(\theta)\ \mathbf{a}^-(\theta)]^T$ contains the beamformer response array (signal lags) in both directions:

$$\mathbf{a}^+(\theta) = \mathbf{a}(-90^\circ) = \left[1, \exp(j\beta^+ d_s), \exp(j\beta^+ 2d_s)\right]^T \tag{A.6}$$

$$\mathbf{a}^-(\theta) = \mathbf{a}(90^\circ) = \left[1, \exp(-j\beta^- d_s), \exp(-j\beta^- 2d_s)\right]^T \tag{A.7}$$

Here d_s is the distance between sensors and $\beta^\pm$ are complex wave numbers corrected for attenuation and mean flow:

$$\beta^+ = \frac{k + \alpha(1-j)}{1+M} \quad \text{and} \quad \beta^- = \frac{k + \alpha(1-j)}{1-M} \tag{A.8}$$

M represents the Mach number, $k = \omega/c$ the acoustic wave number and α the viscothermal attenuation coefficient, which can be computed as:

$$\alpha = \frac{1}{r\,a}\left(\frac{\nu\,\omega}{2}\right)^{1/2}\left[1 - (\gamma - 1)P_r^{-0.5}\right] \tag{A.9}$$

The radius of the duct is denoted by r, a is the speed of sound, ν the cinematic viscosity, $\omega = 2\pi f_k$ the angular frequency and P_r is the Prandtl number.

References

[1] J. O. de Beeck, J. Thompson, N. Booth, Upcoming emission regulations for passenger cars: Impact on scr system requirements and developments, SAE Technical Paper 2013-01-1072. doi:10.4271/2013-01-1072.

[2] C. J. da Silveira Brizon, E. B. Medeiros, Combining subjective and objective assessments to improve acoustic comfort evaluation of motor cars, Applied Acoustics 73 (9) (2012) 913–920. doi:10.1016/j.apacoust.2012.03.013.

[3] F. Schumann, F. Sarikoc, S. Buri, H. Kubach, U. Spicher, Potential of spray-guided gasoline direct injection for reduction of fuel consumption and simultaneous compliance with stricter emissions regulations, International Journal of Engine Research 14 (1) (2013) 80–91. doi:10.1177/1468087412451695.

[4] H. Stoffels, M. Schroeer, NVH Aspects of a Downsized Turbocharged Gasoline Powertrain with Direct Injection, SAE Technical Paper 2003-01-1664. doi:10.4271/2003-01-1664.

[5] C. Teng, S. Homco, Investigation of Compressor Whoosh Noise in Automotive Turbochargers, SAE Int. J. of Passeng. Cars-Mech. Syst. 2 (1) (2009) 1345–1351. doi:10.4271/2009-01-2053.

[6] A. González, M. Ferrer, M. De Diego, G. Piñero, J. Garcia-Bonito, Sound quality of low-frequency and car engine noises after active noise control, Journal of Sound and Vibration 265 (3) (2003) 663–679. doi:10.1016/S0022-460X(02)01462-1.
[7] G. Gaudé, T. Lefèvre, R. Tanna, K. Jin, T. J. B. McKitterick, S. Armenio, Experimental and computational challenges in the quantification of turbocharger vibro-acoustic sources, in: Proceedings of the 37th International Congress and Exposition on Noise Control Engineering (INTER-NOISE 2008), Vol. 2008, Institute of Noise Control Engineering, 2008, pp. 5754–5767.
[8] H. Tiikoja, H. Rämmal, M. Abom, H. Boden, Investigations of automotive turbocharger acoustics, SAE International Journal of Engines 4 (2) (2011) 2531–2542. doi:10.4271/2011-24-0221.
[9] N. Figurella, R. Dehner, A. Selamet, K. Tallio, K. Miazgowicz, R. Wade, Noise at the mid to high flow range of a turbocharger compressor, in: INTER-NOISE and NOISE-CON Congress and Conference Proceedings, Vol. 2012, Institute of Noise Control Engineering, 2012, pp. 8127–8138.
[10] L. Mongeau, D. Thompson, D. McLaughlin, Sound generation by rotating stall in centrifugal turbomachines, Journal of Sound and Vibration 163 (1) (1993) 1 – 30. doi:10.1006/jsvi.1993.1145.
[11] L. Mongeau, D. Thompson, D. Mclaughlin, A method for characterizing aerodynamic sound sources in turbomachines, Journal of Sound and Vibration 181 (3) (1995) 369–389. doi:10.1006/jsvi.1995.0146.
[12] Piñero G. and Vergara, L. and Desantes, J. M. and Broatch, A., Estimation of velocity fluctuation in internal combustion engine exhaust systems through beamforming techniques, Measurement Science & Technology 11 (11) (2000) 1585–1595. doi:10.1088/0957-0233/11/11/307.
[13] C. L. Morfey, Sound transmission and generation in ducts with flow, Journal of Sound and Vibration 14 (1) (1971) 37–55. doi:10.1016/0022-460X(71)90506-2.
[14] E. Dokumaci, On calculation of acoustic power, Journal of Sound and Vibration 238 (5) (2000) 869–876. doi:10.1006/jsvi.2000.3138.
[15] K. Holland, P. Davies, The measurement of sound power flux in flow ducts, Journal of Sound and Vibration 230 (4) (2000) 915–932. doi:10.1006/jsvi.1999.2656.
[16] J. Y. Chung, D. A. Blaser, Transfer function method of measuring acoustic intensity in a duct system with flow, The Journal of the Acoustical Society of America 68 (6) (1980) 1570–1577. doi:http://dx.doi.org/10.1121/1.385211.
[17] P. Davies, Practical flow duct acoustics, Journal of Sound and Vibration 124 (1) (1988) 91 – 115. doi:10.1016/S0022-460X(88)81407-X.
[18] B. Van Veen, K. Buckley, Beamforming: A versatile approach to spatial filtering, ASSP Magazine, IEEE 5 (2) (1988) 4–24. doi:10.1109/53.665.
[19] J. Piper, Broadband beamforming, in: OCEANS 2011, IEEE, 2011, pp. 1–4.
[20] A. Torregrosa, A. Broatch, V. Bermudez, I. Andres, Experimental assessment of emission models used for ic engine exhaust noise prediction, Experimental Thermal and Fluid Science 30 (2) (2005) 97–107. doi:10.1016/j.expthermflusci.2005.05.001.
[21] A. P. Dowling, J. E. F. Williams, Sound and Sources of Sound, Ellis Horwood publishers, 1983.
[22] M. Åbom, H. Bodén, Error analysis of two-microphone measurements in ducts with flow, Journal of the Acoustical Society of America 83 (6) (1988) 2429–2438. doi:10.1121/1.396322.
[23] A. F. Seybert, Two-sensor methods for the measurement of sound intensity and acoustic properties in ducts, Journal of the Acoustical Society of America 83 (6) (1988) 2233–2239. doi:10.1121/1.396352.
[24] L. J. Eriksson, Higher order mode effects in circular ducts and expansion chambers, Journal of the Acoustical Society of America 68 (1980) 545. doi:10.1121/1.384768.
[25] T. Raitor, W. Neise, Sound generation in centrifugal compressors, Journal of Sound and Vibration 314 (2008) 738 – 756. doi:10.1016/j.jsv.2008.01.034.
[26] F. Payri, J. Desantes, A. Broatch, Modified impulse method for the measurement of the frequency response of acoustic filters to weakly nonlinear transient excitations, Journal of the Acoustical Society of America 107 (2) (2000) 731–738. doi:10.1121/1.428256.
[27] J. Galindo, J. R. Serrano, C. Guardiola, C. Cervelló, Surge limit definition in a specific test bench for the characterization of automotive turbochargers, Experimental Thermal and Fluid Science 30 (5) (2006) 449–462. doi:10.1016/j.expthermflusci.2005.06.002.
[28] J. Galindo, A. Tiseira, F. J. Arnau, R. Lang, On-engine measurement of turbocharger surge limit, Experimental Techniques 37 (1) (2013) 47–54. doi:10.1111/j.1747-1567.2010.00697.x.
[29] J. Galindo, H. Climent, C. Guardiola, A. Tiseira, On the effect of pulsating flow on surge margin of small centrifugal compressors for automotive engines, Experimental Thermal and Fluid Science 33 (8) (2009) 1163–1171. doi:10.1016/j.expthermflusci.2009.07.006.
[30] D. Evans, A. Ward, Minimizing Turbocharger Whoosh Noise for Diesel Powertrains, SAE Technical Paper 2005-01-2485. doi:10.4271/2005-01-2485.
[31] D. Evans, A. Ward, The reduction of turbocharger whoosh noise, in: 8^{th} International Conference on Turbochargers and Turbocharging, IMechE, 2006.
[32] C. Sevginer, M. Arslan, N. Sonmez, S. Yilmaz, Investigation of turbocharger related whoosh and air blow noise in a diesel powertrain, in: Proceedings of the 36th International Congress and Exposition on Noise Control Engineering (INTER-NOISE 2007), 2007, pp. 476–485.
[33] I. Frost, O.L., An algorithm for linearly constrained adaptive array processing, Proceedings of the IEEE 60 (8) (1972) 926–935. doi:10.1109/PROC.1972.8817.
[34] A. Hynninen, M. Åbom, Determination of in-duct sound power beyond the plane wave range using wall-mounted microphones, Applied Acoustics 99 (2015) 24 – 30. doi:10.1016/j.apacoust.2015.05.003.
[35] A. Torregrosa, A. Broatch, R. Navarro, J. García-Tíscar, Acoustic characterization of automotive turbocompressors, International Journal of Engine Research 16 (1) (2015) 31–37. doi:10.1177/1468087414562866.
[36] J. Galindo, F. Arnau, A. Tiseira, R. Lang, H. Lahjaily, T. Gimenes, Measurement and modeling of compressor surge on engine test bench for different intake line configurations, SAE Technical Paper (2011-01-0370). doi:10.4271/2011-01-0370.
[37] J. R. Serrano, X. Margot, A. Tiseira, L. M. García-Cuevas, Optimization of the inlet air line of an automotive turbocharger, International Journal of Engine Research 14 (1) (2013) 92–104. doi:10.1177/1468087412449085.
[38] A. Broatch, J. Galindo, R. Navarro, J. García-Tíscar, Methodology for experimental validation of a cfd model for predicting noise generation in centrifugal compressors, International Journal of Heat and Fluid Flow.doi:10.1016/j.ijheatfluidflow.2014.06.006.
[39] R. Kabral, H. Rammal, M. Åbom, Acoustical methods for investigating turbocharger flow instabilities, SAE Technical Paper 2013-01-1879.

doi:10.4271/2013-01-1879.
[40] A. Broatch, J. Galindo, R. Navarro, J. García-Tíscar, A. Daglish, R. Sharma, Simulations and measurements of automotive turbocharger compressor whoosh noise, Engineering Applications of Computational Fluid Mechanics 9 (1) (2015) 12–20. doi:10.1080/19942060.2015.1004788.
[41] I. Andrés, Contribución al estudio y caracterización de la generación de ruido de flujo en el sistema de escape (in spanish), Ph.D. thesis, Universidad Politécnica de Valencia (2003). doi:10.4995/Thesis/10251/2622.